

**Finite-size effects on fragmentation in heavy-ion collisions**Cheng Li,<sup>1,2</sup> Junlong Tian,<sup>2,\*</sup> Li Ou,<sup>1</sup> and Ning Wang<sup>1,†</sup><sup>1</sup>*Department of Physics, Guangxi Normal University, Guilin 541004, People's Republic of China*<sup>2</sup>*School of Physics and Electrical Engineering, Anyang Normal University, Anyang 455000, People's Republic of China*

(Received 24 December 2012; revised manuscript received 29 April 2013; published 28 June 2013)

To investigate the influence of nuclear finite-size effects on the fragmentation in heavy-ion collisions, the fragment charge distributions of  $^{40}\text{Ca} + ^{40}\text{Ca}$ ,  $^{197}\text{Au} + ^{197}\text{Au}$ ,  $^{120}\text{Xe} + ^{129}\text{Sn}$ , and  $^{58}\text{Ni} + ^{48}\text{Ca}$  at intermediate incident energies are studied by using the improved quantum molecular dynamics model. Both the width of the wave packet at the coordinate space and the surface energy term strongly affect the formation and stability of fragments at intermediate-low energies. The wave-packet width influences the stability and the central densities of the initial nuclei. With increase of incident energies, the influence of the detail in description of individual nucleons and of their interaction via mean field on the fragment distributions weakens gradually.

DOI: [10.1103/PhysRevC.87.064615](https://doi.org/10.1103/PhysRevC.87.064615)

PACS number(s): 25.70.Mn, 24.10.Cn, 24.60.Ky

**I. INTRODUCTION**

The heavy-ion nuclear reaction at low and intermediate energies has been studied for many years both theoretically and experimentally [1–8]. In the heavy-ion collisions at incident energies around the Coulomb barrier, the mean field plays a dominant role. One observes particle evaporation, fission, or quasifission of the compound system in the fusion process [9]. The nuclear structure effect such as the surface diffuseness of nuclei and the shell corrections directly influences the Coulomb barrier height and the fusion path. With increasing of incident energies, the nucleon-nucleon collision and fluctuation effect significantly influence the reaction process in addition to the mean-field effect, the mechanism of reaction gradually changes to a multifragmentation process, which is quite different from that at low energies. It is not yet very clear how the nuclear finite-size effects and the dynamical fluctuations affect the reaction process at intermediate incident energies.

To consider the dynamical process in heavy-ion collisions at low and intermediate energies, some microscopic dynamics models, such as the time-dependent Hartree-Fock (TDHF) model [10,11], the Boltzmann-Uehling-Uhlenbeck (BUU) model [12–14], and the improved quantum molecular dynamics (ImQMD) model [15,16] have been developed. The ImQMD model is a semiclassical microscopic dynamics model and is successfully applied on heavy-ion fusion reactions and intermediate energy heavy-ion collisions [15–18]. In the ImQMD model, each nucleon is described by a coherent state of a Gaussian wave packet as that in the traditional quantum molecular dynamics (QMD) model. The width of the wave packet in coordinate space represents the interaction range between nucleons. It influences the structure and stability of an individual nucleus [15]. For heavy-ion collisions at intermediate and high energies, the wave-packet width is usually set as a fixed parameter during the QMD simulations [19,20]. For reactions at intermediate-high energies, a time

evolution of a few hundreds fm/c might be enough to study the reaction process. However, for heavy-ion reactions at energies around the Coulomb barrier, one usually needs a time evolution of several thousands fm/c or even longer to explore the reaction dynamics. To extend the application of the QMD model at low incident energies, it is found that the mass dependence of wave-packet width is required for a better description of the initial nuclei in heavy-ion fusion reactions at energies around the Coulomb barrier [15,16]. In different versions of QMD calculations with different parameter sets, one adopts different values of wave-packet width for better descriptions of heavy-ion reactions at different energies. It is therefore interesting to investigate the influence of the wave-packet width on heavy-ion collisions at different energies. The wave-packet width directly influences the density distribution of the initial nuclei. The surface energy term in the ImQMD model also affects the density distribution of an individual nucleus. For a finite system of nucleus, the surface effect also plays a role for the stability of the initial nuclei. In addition, it was thought that the surface energy of hot fragments produced in multifragmentation reactions differs from the values extracted for isolated nuclei at low excitation based on the calculations of the statistical multifragmentation model [21]. Both the wave packets and the surface energy term influence the properties of nuclear surface and represent the finite-size effects of nuclei. One expects that both of them affect the formation of fragments in heavy-ion collisions. It is therefore necessary to investigate the influence from the wave packets and the surface energy term individually. To study these effects on the formation and stability of the fragments in heavy-ion collisions, we explore the fragment distribution in the reactions  $^{40}\text{Ca} + ^{40}\text{Ca}$ ,  $^{120}\text{Xe} + ^{129}\text{Sn}$ , and  $^{197}\text{Au} + ^{197}\text{Au}$  at intermediate incident energies with the ImQMD model by adopting different wave-packet widths and different surface energy coefficients.

The paper is organized as follows. In Sec. II, we briefly introduce the ImQMD model and show some calculated charge distribution of fragments for  $^{40}\text{Ca} + ^{40}\text{Ca}$ ,  $^{120}\text{Xe} + ^{129}\text{Sn}$ , and  $^{197}\text{Au} + ^{197}\text{Au}$ . In Sec. III, the influence of the different wave-packet widths and the surface energy term on the charge distribution of fragments for  $^{40}\text{Ca} + ^{40}\text{Ca}$  and  $^{197}\text{Au} + ^{197}\text{Au}$  reaction is investigated and the charge and isotope distributions

\* tianjunlong@gmail.com

† wangning@gxnu.edu.cn

TABLE I. Parameter set IQ3 [25] for the ImQMD model.

$\alpha$ (MeV)	$\beta$ (MeV)	$\gamma$	$g_0$ (MeV fm <sup>2</sup> )	$g_\tau$ (MeV)	$\eta$	$C_s$ (MeV)	$\kappa_s$ (fm <sup>2</sup> )	$\rho_0$ (fm <sup>-3</sup> )	$\sigma_0$ (fm)	$\sigma_1$ (fm)
-207	138	7/6	18.0	14.0	5/3	32.0	0.08	0.165	0.94	0.018

for  $^{58}\text{Ni} + ^{48}\text{Ca}$  are predicted. Finally a summary is given in Sec. IV.

## II. MODEL AND SOME TESTS

In the ImQMD model, the same as in the original QMD model [22], each nucleon is represented by a coherent state of a Gaussian wave packet. Through a Wigner transformation, one can get the one-body phase space distribution function for  $N$  distinguishable particles. The nuclear interaction potential energy  $U_{\text{loc}}$  is obtained from the integration of the Skyrme energy density functional  $V_{\text{loc}}[\rho(\mathbf{r})]$ ,

$$V_{\text{loc}} = \frac{\alpha}{2} \frac{\rho^2}{\rho_0} + \frac{\beta}{\gamma + 1} \frac{\rho^{\gamma+1}}{\rho_0^\gamma} + \frac{g_0}{2\rho_0} (\nabla\rho)^2 + \frac{C_s}{2\rho_0} [\rho^2 - \kappa_s (\nabla\rho)^2] \delta^2 + g_\tau \frac{\rho^{\eta+1}}{\rho_0^\eta},$$

which is as the same as that in Refs. [23,24].  $\delta = (\rho_n - \rho_p)/(\rho_n + \rho_p)$  is the isospin asymmetry.  $\rho_n$  and  $\rho_p$  are

the neutron and proton density, respectively. The density distribution  $\rho = \rho_n + \rho_p$  of a system is expressed as

$$\rho(\mathbf{r}) = \sum_i \frac{1}{(2\pi\sigma_r)^{3/2}} \exp\left[-\frac{(\mathbf{r} - \mathbf{r}_i)^2}{2\sigma_r^2}\right]. \quad (1)$$

$\sigma_r$  denotes the width of the wave packet for nucleons in coordinate space. To describe the fermionic nature of the  $N$ -body system and to improve the stability of an individual nucleus, the phase space occupation constraint method and the system-size-dependent wave-packet width (which will be discussed in the next section) are adopted in the ImQMD model. It is found that the phase space occupation constraint is an effective approach to improve the momentum distribution of nuclear system [15,16]. In this work, we adopt the parameter set IQ3 [25] (see Table I), which was applied in the study of heavy-ion fusion reactions at incident energies around the Coulomb barriers.

We first test the ImQMD model for the description of heavy-ion collisions at intermediate energies. The collision reactions for  $^{40}\text{Ca} + ^{40}\text{Ca}$ ,  $^{120}\text{Xe} + ^{129}\text{Sn}$ , and  $^{197}\text{Au} + ^{197}\text{Au}$

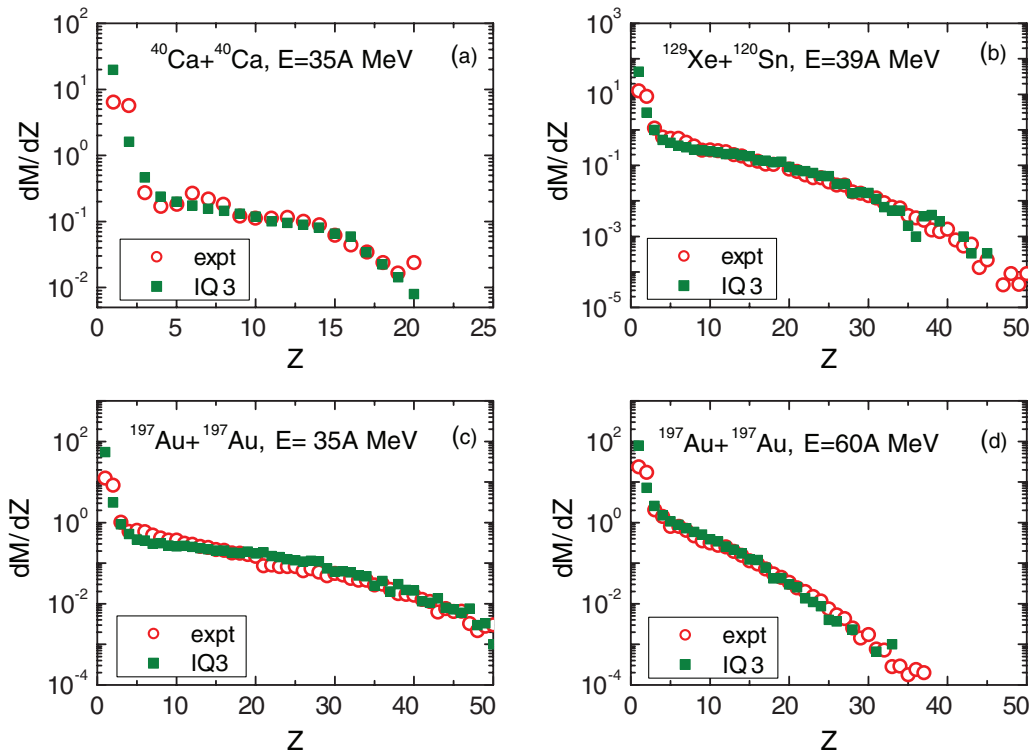


FIG. 1. (Color online) Fragment charge distributions for central collisions of  $^{40}\text{Ca} + ^{40}\text{Ca}$  at incident energy of 35A MeV,  $^{120}\text{Xe} + ^{129}\text{Sn}$  at 39A MeV and  $^{197}\text{Au} + ^{197}\text{Au}$  at 35, 60A MeV. The solid squares and open circles denote the results of the ImQMD model and the experimental data, respectively.

are simulated by using the ImQMD model with the IQ3. Figure 1 shows the charge distribution of fragments for  $^{40}\text{Ca} + ^{40}\text{Ca}$ ,  $^{120}\text{Xe} + ^{129}\text{Sn}$ , and  $^{197}\text{Au} + ^{197}\text{Au}$ . The solid squares and open circles denote the calculation results with the ImQMD model and the experimental data, respectively. Here we create 500 events at each impact parameter  $b$  for the central collisions ( $b = 1 - 3$  fm). For each event, we simulate the whole collision process until  $t = 3000$  fm/c with a step size of  $\Delta t = 1$  fm/c. From Fig. 1, one can see that the charge distribution of fragments calculated by using the ImQMD model with the parameter set IQ3 are in good agreement with the experimental data [26–29]. This indicates that the parameter set IQ3 is also applicable for the study of heavy-ion collisions at intermediate energies.

### III. INFLUENCE OF WAVE-PACKET WIDTH AND SURFACE ENERGY TERM ON MULTIFRAGMENTATION

In the ImQMD model, the mass dependence of the wave-packet width is introduced to consider the nuclear stability of initial nuclei [15],

$$\sigma_r^n = \sigma_0 + \sigma_1 A_n^{1/3}, \quad n = \{p, t\}. \quad (2)$$

Here,  $\sigma_r^p$  ( $\sigma_r^t$ ) denotes the width of wave packet in the coordinate space for the nucleons, which belong to the initial projectile (target) nuclei.  $A_p$  and  $A_t$  denote the mass number of the projectile and target, respectively. For symmetric reaction systems, we set the constant parameter  $\sigma_r = \sigma_r^p = \sigma_r^t$  for all nucleons. The parameters  $\sigma_0$  and  $\sigma_1$  have been listed in Table I. The corresponding values of  $\sigma_r$  are 1.00 and 1.04 fm for  $^{40}\text{Ca}$

and  $^{197}\text{Au}$ , respectively. The stability of the reaction partners plays an important role in heavy-ion reactions, especially for reactions at low incident energies. We find that the wave-packet width strongly affects the stability of the reaction partners after a few hundreds fm/c during the time evolution. It is therefore necessary to investigate the influence of the wave-packet width on the reaction yields.

In this work, we first study the influences of wave-packet width on the stability of nuclei at their ground state and the charge distribution of fragments in heavy-ion collisions, based on the parameter set IQ3 but changing the wave-packet width by adjusting the value of  $\sigma_0$ . Figures 2(a) and 2(b) show the average number of emitted nucleons from the ground-state nuclei  $^{40}\text{Ca}$  and  $^{197}\text{Au}$  at 3000 fm/c as a function of wave-packet width. Here, we create 100 events for each individual nucleus. One sees that the “spurious” emission number of nucleons sharply increases with the decrease of the wave-packet width when  $\sigma_r < 1$  fm. A relatively large wave-packet width helps to improve the stability of nuclei. Figures 2(c) and 2(d) show the central density of the ground-state nuclei  $^{40}\text{Ca}$  and  $^{197}\text{Au}$  at the time of  $t = 500$  fm/c. One can see that the central density increases with the wave-packet width. Too large wave-packet width causes the central densities to be obviously higher than the normal density, which is about  $0.165 \text{ fm}^{-3}$ . This means that a suitable wave-packet width is needed to fulfill both the stability and the central density requirements. A reasonable density distribution for the reaction partners is helpful for a reasonable description of the fragmentation in heavy-ion collisions at low and intermediate energies.

In Fig. 3, we present the charge distribution of fragments for central collisions of  $^{40}\text{Ca} + ^{40}\text{Ca}$  and  $^{197}\text{Au} + ^{197}\text{Au}$  at

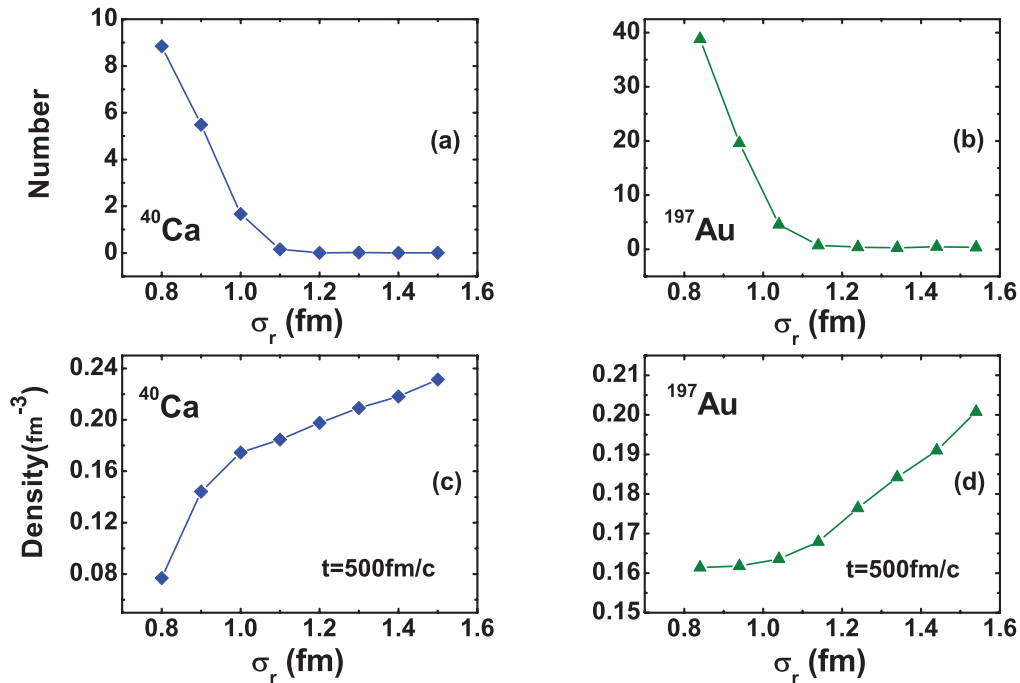


FIG. 2. (Color online) Upper panels: Average number of emitted nucleons from the ground-state nuclei of  $^{40}\text{Ca}$  and  $^{197}\text{Au}$  at  $t = 3000$  fm/c with different wave-packet width. Lower panels: Central density of the ground-state nuclei of  $^{40}\text{Ca}$  and  $^{197}\text{Au}$  at  $t = 500$  fm/c.

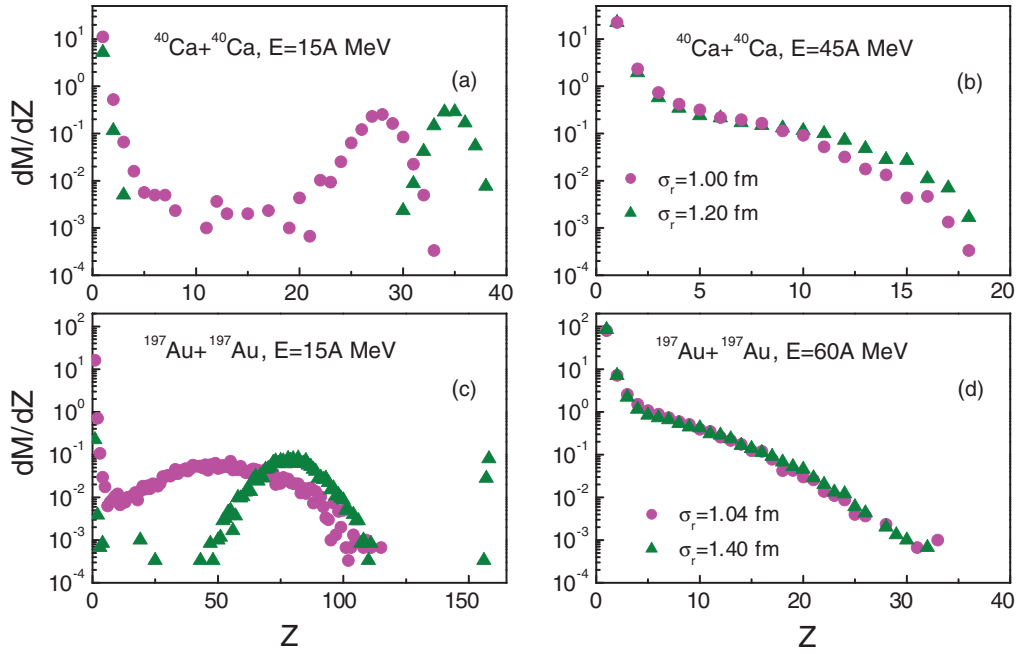


FIG. 3. (Color online) Charge distributions of fragments of  $^{40}\text{Ca} + ^{40}\text{Ca}$  and  $^{197}\text{Au} + ^{197}\text{Au}$  at low and intermediate energies with different wave-packet width.

intermediate incident energies with different wave-packet widths. From Figs. 3(a) and 3(c), an obvious discrepancy due to adopting different wave-packet widths for the charge distribution of fragments in  $^{40}\text{Ca} + ^{40}\text{Ca}$  and  $^{197}\text{Au} + ^{197}\text{Au}$  at an incident energy of 15A MeV can be observed. We note that the peak position of the charge distribution of heavy fragments increases with increasing of the wave-packet width, and the yield of light and intermediate mass fragments ( $2 \leq Z \leq 30$ ) with  $\sigma_r = 1.20$  fm is much lower than that with  $\sigma_r = 1.00$  fm in Fig. 3(a). From Fig. 3(c), one sees that the peak positions of the charge distribution of fragments for  $^{197}\text{Au} + ^{197}\text{Au}$  are approximately located at around  $Z = 50$  and 80 with  $\sigma_r = 1.04$  and 1.40 fm, respectively. There exists a few superheavy fragments with charge number  $Z > 150$  if one takes  $\sigma_r = 1.40$  fm. This is because a larger wave-packet width causes the composite system to be bound too tightly and inhibits the breakup of the heavy system. In the ImQMD model, the widths of wave packets in coordinate space and those in momentum space satisfy the minimum uncertainty relation. A relatively small value for  $\sigma_r$  implies that the uncertainty of momentum of particle is relatively large which brings more dynamical fluctuations in reactions.

One can also see from Figs. 3(b) and 3(d) that the results of  $^{40}\text{Ca} + ^{40}\text{Ca}$  and  $^{197}\text{Au} + ^{197}\text{Au}$  do not change appreciably by taking different wave-packet widths at a relatively higher energy especially for the reaction  $^{197}\text{Au} + ^{197}\text{Au}$ . This implies that the influence of wave-packet width on the charge distribution of fragments in heavy-ion collisions gradually weakens with the increase of the incident energies. It is known that the mean field plays a dominant role in low-energy reactions, and the wave-packet width mainly influences the mean-field effect. However, for reactions at intermediate energies the contribution of nucleon-nucleon collisions increases

with the increasing of incident energy, and the influence of nucleon-nucleon interactions via mean field gradually weakens.

The surface energy term is represented as

$$U_{\text{surf}} = \frac{g_0}{2} \int (\nabla \rho)^2 d^3r \quad (3)$$

in the ImQMD model, where  $g_0$  is the surface energy coefficient. Figure 4 shows the time evolution of a typical event for the ground-state nuclei  $^{197}\text{Au}$  and  $^{90}\text{Zr}$  without the surface energy term being considered (i.e.,  $g_0 = 0$ ). The  $^{197}\text{Au}$  nucleus spontaneously splits into two fragments after  $t = 700$  fm/c if the surface energy term is not involved. For  $^{90}\text{Zr}$ , the nucleus does not breakup before  $t = 3000$  fm/c. This indicates that the Coulomb repulsion can result in the breakup of heavy nucleus if the surface term is removed like that in the liquid-drop model. We also note that the central densities of nuclei do not obviously change by varying the surface energy coefficient, which is different from the influence of the wave-packet width.

For studying the effects of the surface energy term on the charge distribution of fragments for heavy-ion collisions, we show the comparison of the charge distribution of fragments for  $^{40}\text{Ca} + ^{40}\text{Ca}$  at the incident energies of 15 and 45A MeV and  $^{197}\text{Au} + ^{197}\text{Au}$  at 15 and 60A MeV with different surface energy coefficients in Fig. 5. The open and solid circles denote the results with the surface energy coefficients  $g_0 = 7$  and 18 MeV fm<sup>2</sup>, respectively. From Figs. 5(a) and 5(c), one sees that the yields of heavy fragments are lower and those of the intermediate mass fragments are higher with  $g_0 = 7$  MeV fm<sup>2</sup> than the case with  $g_0 = 18$  MeV fm<sup>2</sup>. These investigations indicate that the formation of fragments in the heavy-ion collisions is closely related to the surface energy

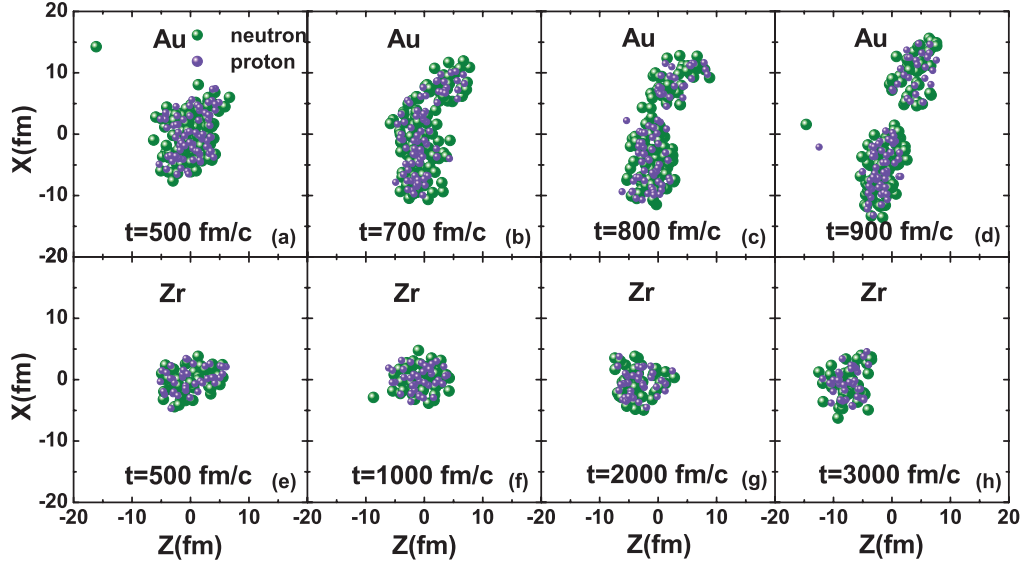


FIG. 4. (Color online) Time evolution of a typical event for the ground state  $^{197}\text{Au}$  and  $^{90}\text{Zr}$  by setting the surface energy coefficient  $g_0 = 0$ .

term, especially for the reactions in low excitation energies. At low energies the evolution of the charge yields predicted by ImQMD (i.e., that nuclei disintegrate into smaller fragments with decreasing surface energy) is similar to the predictions of a statistical model of Ref. [21]. The surface energy term inhibits the breakup of heavy nucleus caused by the Coulomb repulsion. If the value of the surface energy coefficient is too small, the formation of heavy fragments in heavy-ion collisions will be suppressed. From Figs. 5(b) and 5(d), one can see that the discrepancy due to different surface energy coefficients

becomes smaller with the increasing of the incident energies.

In Fig. 6(a), we show the predicted fragment charge distributions for central collisions of  $^{58}\text{Ni} + ^{48}\text{Ca}$  at the incident energies of 25 and 35A MeV with the ImQMD model by using the parameter set IQ3. Here we create 1000 events at each impact parameter for the central collisions. For each event, we directly simulate the whole collision process until  $t = 3000$  fm/c without combining the statistical model. For the collisions at energies around 25A MeV, the competition

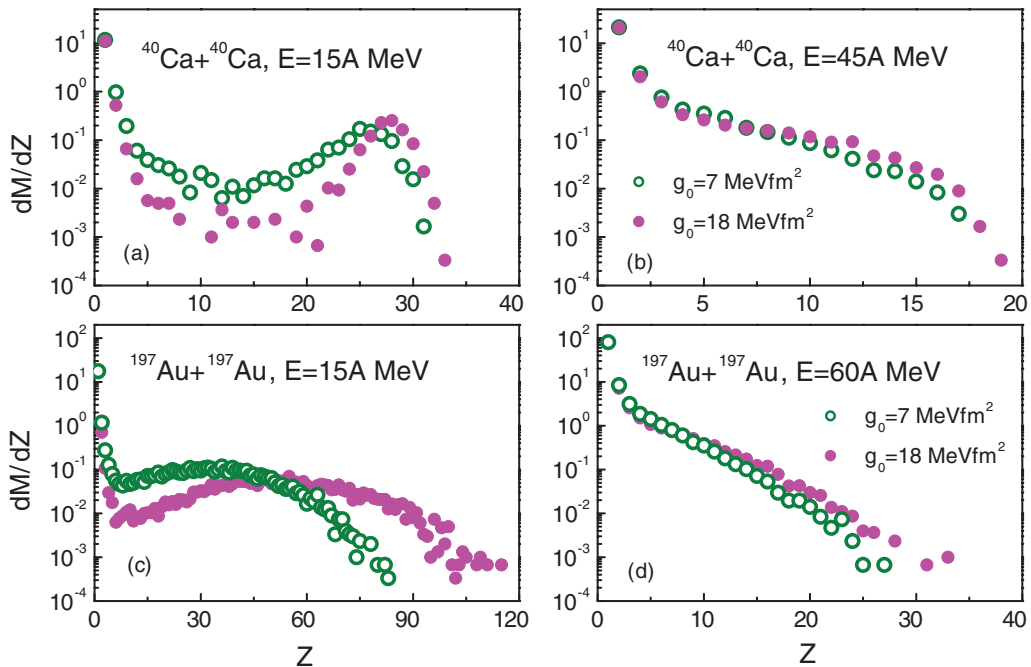


FIG. 5. (Color online) Charge distributions of fragments for  $^{40}\text{Ca} + ^{40}\text{Ca}$  and  $^{197}\text{Au} + ^{197}\text{Au}$  with different surface energy coefficients. The open and solid circles denote the results with the surface energy coefficient  $g_0 = 7$  and  $18 \text{ MeV fm}^2$ , respectively.

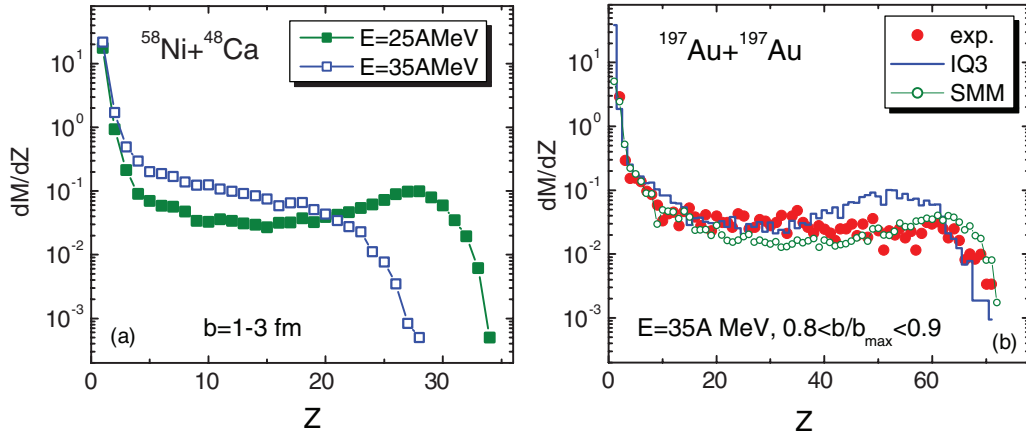


FIG. 6. (Color online) Calculated fragment charge distributions for (a) central collisions of  $^{58}\text{Ni} + ^{48}\text{Ca}$  at incident energies of 25 and 35 A MeV and (b) peripheral collisions of  $^{197}\text{Au} + ^{197}\text{Au}$  at  $E = 35\text{A MeV}$ , with the ImQMD model by using the parameter set IQ3. The experimental data for the mean elemental event multiplicity [30] and the corresponding results of the statistical multifragmentation model (SMM) [30] are also presented for comparison in (b).

between fusion-fission and multifragmentation is expected. If the statistical model is further combined for the description of the fusion-fission process of the composite system, the peak of the charge distribution at  $Z \approx 28$  in the collisions with  $E = 25\text{A MeV}$  could be reduced.

To further analyze the influence of the competition between fission and multifragmentation at relatively lower excitation energies, the peripheral collisions of  $^{197}\text{Au} + ^{197}\text{Au}$  at incident energy of 35 A MeV are also investigated. In addition to central collisions, the peripheral collisions of heavy-ion reactions at

intermediate energies are also helpful to test the dynamical and statistical models [21]. From Fig. 6(b), we find that the ImQMD calculations just qualitatively describe the experiment data (after a running time of 3000 fm/c) in the peripheral collisions of  $^{197}\text{Au} + ^{197}\text{Au}$ , although the central collisions of this reaction at the same incident energy (see Fig. 1) can be described reasonably well. It is known that for heavy-ion reactions at the same incident energy the excitation energies of the composite system in peripheral collisions are relatively lower than those in the central collisions. The competition

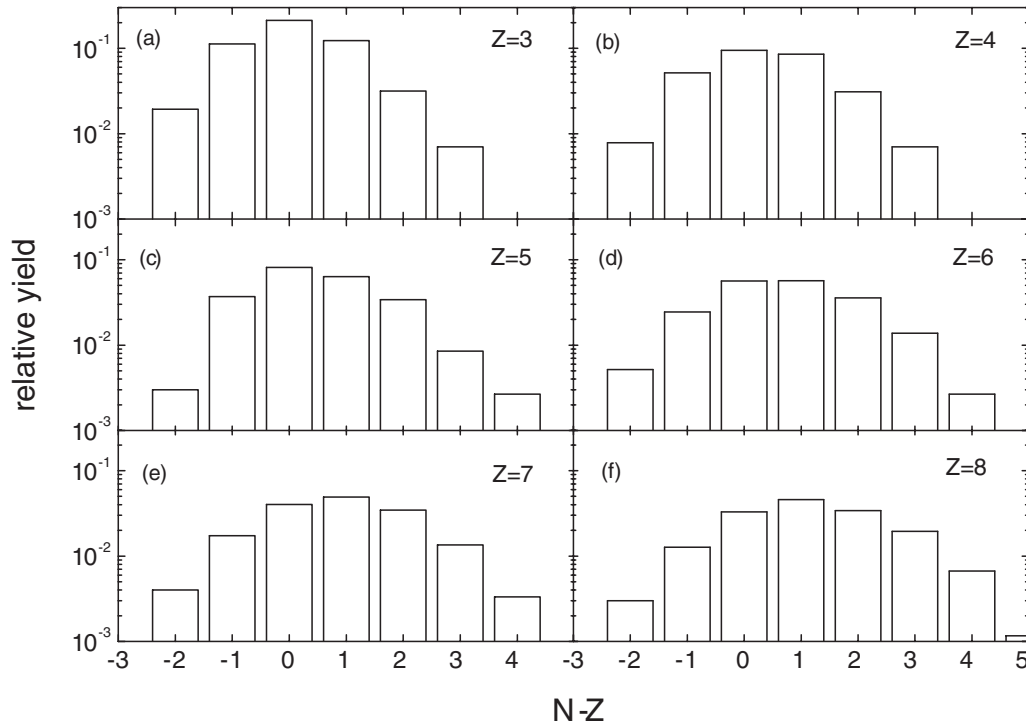


FIG. 7. Isotope distributions for central collisions of  $^{58}\text{Ni} + ^{48}\text{Ca}$  at incident energies of 35 A MeV with IQ3.  $N$  and  $Z$  denote the neutron and proton number of fragments, respectively.

between evaporation, fission, and multifragmentation at the relatively lower excitation energies becomes important and the statistical model should be combined for a better description of the secondary deexcitation of primary hot fragments. One expects that the charge distribution for heavy fragments in peripheral collisions of  $^{197}\text{Au} + ^{197}\text{Au}$  could be improved when the statistical model is further combined. The results of the statistical multifragmentation model (SMM) [30] are also presented for comparison. The charge distribution especially for heavy fragments can be reasonably well reproduced with the SMM calculations. The ImQMD simulations are helpful for the study of the competition, since the time scale for the fusion-fission process is much longer than that for the multifragmentation process. In Fig. 7, we show the predicted isotope distribution for central collisions of  $^{58}\text{Ni} + ^{48}\text{Ca}$  at incident energies of 35A MeV by using the ImQMD model with IQ3. For light fragments, the predicted yields for nearly symmetric fragments are relatively high due to the influence of nuclear symmetry energy. One should note that the secondary deexcitation process, which is usually described by using the statistical model [30,31], could further change the calculated isotope distribution in Fig. 7.

#### IV. SUMMARY

The influence of nuclear finite-size effects on the formation and stability of fragments in heavy-ion collisions at low and intermediate energies has been investigated by using the improved quantum molecular dynamics model. We find that a suitable wave-packet width is needed to fulfill both the stability and central density requirements. Too small wave-packet width breaks the stability of initial nuclei through carrying more dynamical fluctuations and too large wave-packet width causes the central densities to be obviously higher than the normal density. The surface energy term is also

important for improving the stability of initial nuclei. It inhibits the breakup of heavy nucleus caused by the Coulomb repulsion. With the parameter set IQ3, the charge distribution of fragments in central collisions of  $^{40}\text{Ca} + ^{40}\text{Ca}$ ,  $^{120}\text{Xe} + ^{129}\text{Sn}$ ,  $^{197}\text{Au} + ^{197}\text{Au}$  are reasonably well reproduced. By using different wave-packet widths and different surface energy coefficients, the charge distribution of fragments for  $^{40}\text{Ca} + ^{40}\text{Ca}$  and  $^{197}\text{Au} + ^{197}\text{Au}$  are simultaneously studied to investigate the influence of nuclear finite-size effect. Both the wave-packet width, which represents the range of nucleon-nucleon interaction, and the surface energy term strongly affect the stability of nuclear system and the yields of fragments in heavy-ion collisions at incident energies of a few MeV/nucleon to several tens MeV/nucleon. With increase of incident energies, the influence of the detail in description of individual nucleons (width of wave-packet) and of their interaction via mean field on the fragment distributions weakens gradually. For heavy reaction systems with relatively low excitation energies, the competition between particle evaporation, fission, and multifragmentation plays an important role for the reaction yields and the statistical model should be further combined even after a running time of several thousands fm/c with the microscopic dynamics simulations for a better description of the secondary deexcitation of primary hot fragments. The study on the combination of the statistical model is a topic for future research.

#### ACKNOWLEDGMENTS

J.T. is grateful to Dr. Ying-Xun Zhang for fruitful discussions. This work was supported by the National Natural Science Foundation of China (Grants No. 11005003, No. 11275052, and No. 11005022) and the Natural Science Foundation of He'nan Educational Committee (Grants No. 2011A140001 and No. 2011GGJS-147).

- 
- [1] L. Shvedov, M. Colonna, and M. Di Toro, *Phys. Rev. C* **81**, 054605 (2010).
  - [2] D. Ardouin, *Int. J. Mod. Phys. E* **6**, 391 (1997).
  - [3] M. Colonna, M. Di Toro, V. Latora, and N. Colonna, *Nucl. Phys. A* **545**, 111 (1992).
  - [4] Z. Seres, F. Deák, A. Kiss, G. Caskey *et al.*, *Nucl. Phys. A* **492**, 315 (1989).
  - [5] R. L. Watson, R. J. Maurer, B. B. Bandong, and C. Can, *Lect. Notes Phys.* **294**, 382 (1988).
  - [6] R. Płaneta, F. Amorini, A. Anzalone *et al.*, *Phys. Rev. C* **77**, 014610 (2008).
  - [7] P. Staszal, Z. Majka, L. G. Sobotka *et al.*, *Phys. Rev. C* **63**, 064610 (2001).
  - [8] R. Wada, K. Hagel, J. Cibor *et al.*, *Phys. Rev. C* **62**, 034601 (2000).
  - [9] N. Wang, K. Zhao, W. Scheid, and X. Wu, *Phys. Rev. C* **77**, 014603 (2008); <http://www.imqmd.com/wangning/hivap2.rar>.
  - [10] C. Golabek and C. Simenel, *Phys. Rev. Lett.* **103**, 042701 (2009).
  - [11] A. S. Umar, V. E. Oberacker, J. A. Maruhn, and P.-G. Reinhard, *EPJ Web Conf.* **17**, 9001 (2011).
  - [12] T. Gaitanos, H. Lenske, and U. Mosel, *Prog. Part. Nucl. Phys.* **62**, 439 (2009).
  - [13] B. A. Li and D. H. E. Gross, *Nucl. Phys. A* **554**, 257 (1993).
  - [14] Li Ou and Bao-An Li, *Phys. Rev. C* **84**, 064605 (2011).
  - [15] N. Wang, Z. X. Li, and X. Z. Wu, *Phys. Rev. C* **65**, 064608 (2002).
  - [16] Y. Jiang, N. Wang, Z. Li, and W. Scheid, *Phys. Rev. C* **81**, 044602 (2010).
  - [17] M. B. Tsang, Y. X. Zhang, P. Danielewicz, M. Famiano, Z. X. Li, W. G. Lynch, and A. W. Steiner, *Phys. Rev. Lett.* **102**, 122701 (2009).
  - [18] J. L. Tian, X. Z. Wu, K. Zhao, Y. X. Zhang, and Z. X. Li, *Phys. Rev. C* **77**, 064603 (2008).
  - [19] C. Hartnack, R. K. Puri, J. Aichelin, J. Konopka *et al.*, *Eur. Phys. J. A* **1**, 151 (1998).
  - [20] S. Kumar and Y. G. Ma, *Phys. Rev. C* **86**, 051601(R) (2012).
  - [21] A. S. Botvina, N. Buyukcizmeci, M. Erdogan, J. Łukasik, I. N. Mishustin, R. Ogul, and W. Trautmann, *Phys. Rev. C* **74**, 044609 (2006).
  - [22] J. Aichelin, *Phys. Rep.* **202**, 233 (1991).
  - [23] N. Wang, Z. Li, X. Wu, J. Tian, Y. X. Zhang, and M. Liu, *Phys. Rev. C* **69**, 034608 (2004).
  - [24] K. Zhao, X. Wu, and Z. Li, *Phys. Rev. C* **80**, 054607 (2009).

- [25] V. Zanganeh, N. Wang, and O. N. Ghodsi, *Phys. Rev. C* **85**, 034601 (2012).
- [26] K. Hagel *et al.*, *Phys. Rev. C* **50**, 2017 (1994).
- [27] K. Hagel, M. Gonin *et al.*, *Phys. Rev. Lett.* **68**, 2141 (1992).
- [28] S. Hudan, A. Chbihi, J. D. Frankland *et al.*, *Phys. Rev. C* **67**, 064613 (2003).
- [29] F. Lavaud, E. Plagnol, G. Auger *et al.*, *AIP Conf. Proc.* **610**, 716 (2002).
- [30] M. D'Agostino, A. S. Botvina, M. Bruno, A. Bonasera, J. P. Bondorf, R. Bougault, P. Désquelles, E. Geraci, F. Gulminelli, I. Iori *et al.*, *Nucl. Phys. A* **650**, 329 (1999).
- [31] J. P. Bondorf, A. S. Botvina, A. S. Iljinov, I. N. Mishustin, and K. Sneppen, *Phys. Rep.* **257**, 133 (1995).